NUCL SCI TECH (2018) 29:186
https://doi.org/10.1007/s41365-018-0523-9

Influence of α-clustering nuclear structure on the rotating collision system

Zhi-Wan Xu[1,2] · **Song Zhang**[3,4] · **Yu-Gang Ma**[3,4] · **Jin-Hui Chen**[3,4] · **Chen Zhong**[3,4]

Received: 20 November 2018 / Revised: 26 November 2018 / Accepted: 26 November 2018 / Published online: 3 December 2018
© China Science Publishing & Media Ltd. (Science Press), Shanghai Institute of Applied Physics, the Chinese Academy of Sciences, Chinese Nuclear Society and Springer Nature Singapore Pte Ltd. 2018

Abstract In recent years, the collective motion properties of global rotation of the symmetric colliding system in relativistic energies have been investigated. In addition, the initial geometrical shape effects on the collective flows have been explored using a hydrodynamical model, a transport model, etc. In this work, we study the asymmetric $^{12}\mathrm{C}+^{197}\mathrm{Au}$ collision at 200 GeV/c and the effect of the exotic nuclear structure on the global rotation using a multi-phase transport model. The global angular momentum and averaged angular speed were calculated and discussed for the collision system at different evolution stages.

This work was supported in part by National Key R&D Program of China (No. 2016YFE0100900), the National Natural Science Foundation of China (Nos. 11421505, 11220101005, 11775288, and U1232206), the Major State Basic Research Development Program in China (No. 2014CB845400), the Key Research Program of Frontier Sciences of the CAS (No. QYZDJ-SSW-SLH002), and the Key Research Program of the Chinese Academy of Sciences (No. XDPB09).

✉ Yu-Gang Ma
ygma@sinap.ac.cn

Song Zhang
zhangsong@sinap.ac.cn

1 Department of Physics, Fudan University, Shanghai 200433, China

2 Department of Physics and Astronomy, University of California, Los Angeles, CA 90095, USA

3 Key Laboratory of Nuclear Physics and Ion-beam Application (MOE), Institute of Modern Physics, Fudan University, Shanghai 200433, China

4 Shanghai Institute of Applied Physics, Chinese Academy of Sciences, Shanghai 201800, China

Keywords Chiral magnetic effect · Chiral vortical effect · Initial geometrical effect · Quark–gluon plasma · Relativistic heavy-ion collisions

1 Introduction

In relativistic heavy-ion collisions, properties of the collision system are often investigated using the identified particle spectra, collective motion in transverse momentum plane (collective flow) [1–4], jet quenching [5, 6], Hanbury–Brown–Twiss (HBT) correlation [7, 8], etc. Many experimental results suggest that hot dense matter at the partonic level with large collective motion is created in the early stages of relativistic heavy-ion collisions; this is a new type of strong-coupling quark–gluon plasma (QGP) matter with almost the nearly lowest shear viscosity.

On the other hand, global rotation of the collision system is important to understand the global and local polarization of the quark matter. By using a multi-phase transport (AMPT) model and hard-sphere model, evolution of angular momentum and vorticity fields has been calculated for Au + Au collisions [9]. Some theoretical works have predicted globally polarized QGP in relativistic heavy-ion collisions [10, 11], and it was suggested that system vorticity and particle production mechanism should be studied by measuring global spin alignment of vector mesons in relativistic heavy-ion collisions [12, 13]. Recently, RHIC-STAR collaboration [14] reported the first measurements for global Λ hyperon polarization in Au + Au collisions, indicating that the vorticity of the QGP might reach $\omega \sim (9 \pm 1) \times 10^{21}$/s, which far surpasses the vorticity of all other known fluids.

The initial geometry distribution could influence initial dynamical fluctuation and intrinsic structure in the collided system, which affects the collective flow, HBT correlation, etc. Hydrodynamical models [15–18] as well as transport models [19–23] were employed to investigate these effects. Some observables or physical quantities that are sensitive to the initial geometry distribution were proposed, such as collective flows [24–26], fluctuation of conserved quantities [27, 28], density fluctuations [29], and charge separation [30]. In references [19, 20], the carbon was considered with a 3-α structure and collided against a heavy nucleus at very high energies; the results implied that the final collective flow was sensitive to the intrinsic geometry distribution of carbon. The ratio of triangular flow to elliptic flow can be used to detect the intrinsic structure of α-clustering nuclei within an α-clustered ^{12}C colliding against heavy ion by using AMPT model [31]. The α-cluster model, which was originally proposed by Gamow [32], considered some light nuclei made of N-α, such as ^{12}C with 3-α and ^{16}O with 4-α. It was suggested that α clustering configurations can be identified by giant dipole resonance [33, 34] or photonuclear reaction in the quasi-deuteron region [35, 36] by an extended quantum molecular dynamics (EQMD) model.

In this work, the angular momentum, inertia, and average angular velocity for an asymmetric collision system, namely ^{12}C$+^{197}$Au, was investigated for comparing the three different clustering configurations of ^{12}C. In the second section, an introduction to AMPT model and the calculation methods for angular momentum and other physical quantities in the many-body system is presented. In the third section, we first discuss the main calculation results of the angular momentum, inertia, and velocity for the three clustering configurations. Then, we explore the density distribution of the system in detail. The paper is concluded in the fourth section.

2 Model and calculation methods

A step-by-step simulation of heavy-ion collisions in phase space was obtained by AMPT model [37]. AMPT is a successful model used to study colliding energy ranges of relativistic heavy-ion collisions at RHIC [37] and LHC [38]. The model can be used to study pion HBT correlations [39], collective flow [40, 41], di-hadron azimuthal correlations [42], strangeness production [28, 43], and chiral magnetic effects [44, 45].

AMPT model was developed to simulate the collision system. It is applied to different transport theories to describe the many-body interaction from the initial to final states. The model is initialized by employing the HIJING model [46, 47] that generated hard mini-jet partons and soft strings to form initial states. It was followed by a parton cascade model (ZPC) [48] that simulates the interaction of the melted partons. Then, a quark coalescence model was adopted to describe the formation of hadrons; these hadrons participate in hadronic rescattering using a relativistic transport (ART) model [49].

The initial nucleon distribution in ^{12}C would be a Woods–Saxon distribution, which originated from the HIJING model [46, 47], or α-cluster configurations [33, 34, 50]. The latter configurations include two cases: the three α-clustering chain structure and the three α-clustering triangle structure. The parameters for the α-clustered ^{12}C were configured from the EQMD model [33, 34, 50] and are discussed in our previous work [31] in detail. Therefore, we can obtain the phase space in ^{12}C$+^{197}$Au collisions at $\sqrt{s_{NN}}$ = 200 GeV for the calculations using AMPT model.

In this work, ^{12}C is configured as a chain structure, triangle structure with 3-α , and the Woods–Saxon distribution of nucleons from the HIJING model [46, 47] packaged in AMPT model. For ^{197}Au, its initial

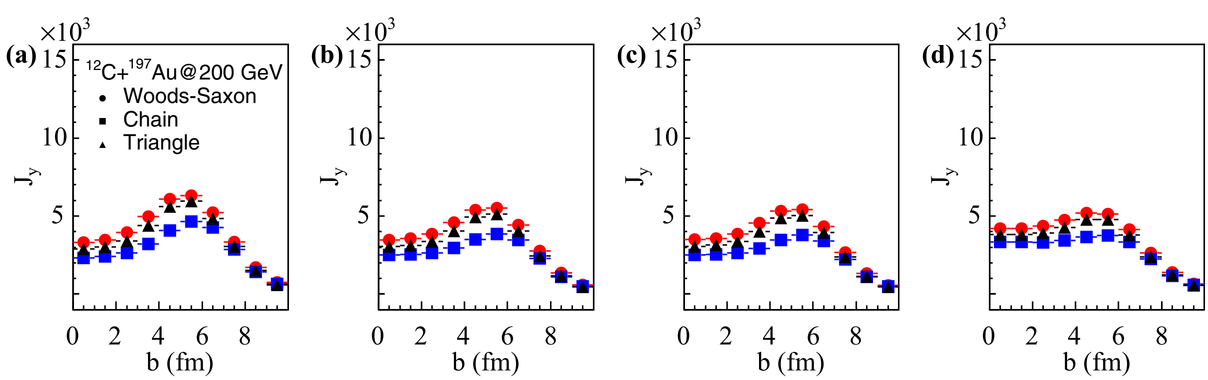

Fig. 1 (Color online) Angular momentum J_y at different impact parameters in the collision process for ^{12}C$+^{197}$Au collision at $\sqrt{s_{NN}} = 200$ GeV. From left to right panel: **a** the initial partons, **b** the freeze-out partons, **c** the hadrons without hadronic rescattering, and **d** the final-state hadrons. The three colors represent the three different α-cluster structures of the ^{12}C. **a** Participant **b** freezed parton **c** h w.o. rescatt **d** h with rescatt

configuration was just the simple Woods–Saxon distribution. The distribution of the radial center of the α clusters in ^{12}C is assumed to be a Gaussian function, $e^{-0.5\left(\frac{r-r_c}{\sigma_{r_c}}\right)^2}$, where r_c is average radial center of an α cluster and σ_{r_c} is the width of the distribution. In addition, the nucleon inside each α cluster will be given by the Woods–Saxon distribution. The parameters of r_c and σ_{r_c} can be obtained using the EQMD calculations [33–36]. For the triangle structure, r_c = 1.8 fm and σ_{r_c} = 0.1 fm. For the chain structure, r_c = 2.5 fm and σ_{r_c} = 0.1 fm for the two outer α clusters, and the other cluster will be at the center in ^{12}C. Once the radial center of the α cluster is determined, the centers of the three clusters will be placed in an equilateral triangle for the triangle structure or in a line for the chain structure. Further details can be found in our previous work [31, 51].

In heavy-ion collisions, impact parameter b is defined as the perpendicular distance between the path center of projectile nucleus and the target nucleus. The plane formed by b and the beam direction is called the reaction plane. Because the direction of b is random for every collision, the reaction plane direction will also be random. Hence, the observables that are sensitive to the reaction plane direction should be corrected to that. The participant plane is considered as the reasonable proximation to the reaction plane, and the participant plane angle $\Psi_n\{PP\}$ is defined by the following equation [52–54]:

$$\Psi_n\{PP\} = \frac{\tan^{-1}\left(\frac{\langle r^2 \sin(n\phi_{\text{part}})\rangle}{\langle r^2 \cos(n\phi_{\text{part}})\rangle}\right) + \pi}{n}, \tag{1}$$

where $\Psi_n\{PP\}$ is the nth-order participant plane angle, r and ϕ_{part} are the coordinate position and azimuthal angle of participants in the collision zone in the initial state, respectively, and the average $\langle \cdots \rangle$ denotes the density weighting. For the calculation, the system will be rotated to the participant plane direction in the transverse plane.

In AMPT model, we consider a many-body system with discrete particles, and the total angular momentum $\vec{J}$ can be calculated by summing each particle's contribution as done for low-energy heavy-ion collisions [55].

$$\vec{J} = \sum_i \vec{r}_i \times \vec{p}_i, \tag{2}$$

where $\vec{r}_i$ and $\vec{p}_i$ are the coordinates and momentum of each particle, respectively. The relation between vorticity $\vec{\omega}_i$ and velocity $\vec{v}_i$ is $\vec{v}_i = \vec{\omega}_i \times \vec{r}_i$ for the particle and $\vec{v}_i = \vec{p}_i/E_i$, where E_i is the particle's energy. In this model, the system is symmetric around the system rotational axis $\hat{\omega}$ with a constant vorticity $\vec{\omega}$. If the system is considered as an approximate rigid body in a fixed stage, each particle's vorticity $\vec{\omega}_i$ has a component projected onto the axis $\hat{\omega}$, namely the $\vec{\omega}$, and the vertical component will cancel each other out within the system. From the above discussion, the angular momentum can be written as

$$\begin{aligned}\vec{J} &= \sum_i \vec{r}_i \times \vec{p}_i \\ &= \sum_i (|\vec{r}_i|^2 \vec{\omega}_i - (\vec{\omega}_i \cdot \vec{r}_i)\vec{r}_i)E_i \\ &= \sum_i (|\vec{r}_i|^2 - (\hat{\omega} \cdot \vec{r}_i)^2)E_i \vec{\omega},\end{aligned} \tag{3}$$

where $I_0 = \sum_i (|\vec{r}_i|^2 - (\hat{\omega} \cdot \vec{r}_i)^2)E_i$ is the moment-of-inertia. Because the phase space of the system is corrected to event plane angle, the event plane direction will be along the y-axis, and $\vec{\omega}$ will also be along the y-axis. The above discussion and deducing are in the assumption of approximate rigid body system, and for the expanding system with discrete particles, the averaged vorticity component along the y-axis can be defined using a similar method from [9] as

$$\langle \omega_y \rangle = \frac{\sum_i (|\vec{r}_i|^2 - (\hat{\omega} \cdot \vec{r}_i)^2)E_i \omega_{i,y}}{I_0}. \tag{4}$$

In the earlier stage, our observation focused on the u($\bar{u}$), d($\bar{d}$), and s($\bar{s}$) quarks, which are primarily composed of partons and therefore implicated most physics in the collision system. After hadronization, the system experiences a phase transfer to later stages; then, we focused on (anti-) protons and other mesons, including $\pi^\pm$ and $K^\pm$. The phases we considered for the transport simulation of the collision are the initial partons, freeze-out partons, hadrons without hadronic rescattering, and final-state hadrons.

3 Results and discussion

For non-central collisions, the total angular momentum of the collision system would be mainly along the y-axis [9], which in the case of ^{12}C + ^{197}Au collision would be of the order of magnitude of 10^5. Most of the total angular momentum was carried by the spectators on the outer edge of the initial nucleus that passed on without being intervened, while the colliding parts, known as the participants, formed the QGP matter under high temperature and pressure [31, 37, 51]. Therefore, because we only considered the participants using Eq. (3), the remnant angular momentum is reduced to the order of magnitude of 10^3, as indicated in Fig. 1a.

From the hydrodynamic perspective, the colliding system was nearly isolated [56, 57]. Therefore, the angular momentum would be conserved during the system evolvement after the collision. From Fig. 1a–d, it can clearly be seen that J_y did not change significantly during the four stages: initialed participants, partons at freeze-out

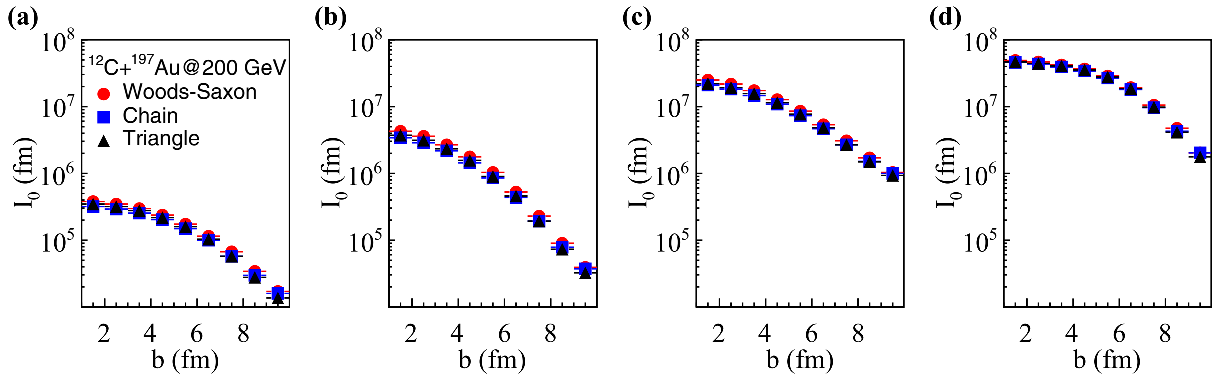

Fig. 2 (Color online) Same as Fig. 1, except for the angular inertia. **a** Participant **b** freezed parton **c** h w.o. rescatt **d** h with rescatt

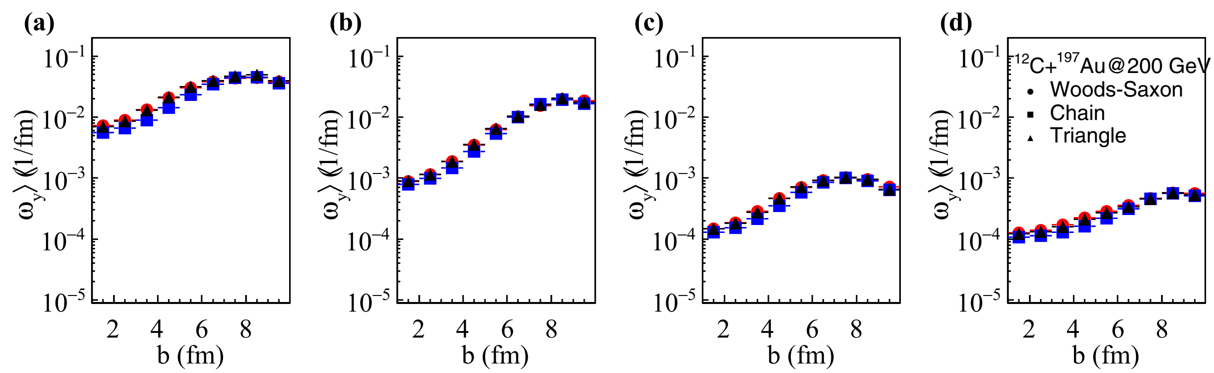

Fig. 3 (Color online) Same as Fig. 1, except for the average angular velocity along the *y*-axis. **a** Participant **b** freezed parton **c** h w.o. rescatt **d** h with rescatt

stage, hadrons without hadron rescattering, and hadrons after hadron rescattering. However, the QGP matter soon cooled down and then froze out, scattering out the particles that had a high momentum [51, 56]. Therefore, the system expanded, and the total angular inertia increased significantly from the order of magnitude of 10^5 to 10^7, which is shown in Fig. 2a–d. On the other hand, the decreasing average angular velocity $\langle \omega_y \rangle$ calculated using Eq. (4) could also manifest the system expansion in Fig. 3, corresponding to the increasing I_0.

In Fig. 1a, the angular momentum of the participants first increased and then decreased when the impact parameter b was increased gradually, which is in agreement with the results of other works [9]. This tendency can be understood from Eq. (2); in near-central collision, the angular momentum was dominated by the distance between each discrete particle and the center of mass, the increase of which contributed to the rising total angular momentum. However, the ^{197}Au nucleus employed the Woods–Saxon distribution [21–23], which possessed the Gaussian density drop against the radius; therefore, fewer initial nucleons (participants) could be contributed to the colliding process as the impact parameter increased. Because ^{12}C occupied a smaller region than ^{197}Au [19, 20], the Woods–Saxon distribution of Au also induced the decreasing tendency of the total angular inertia at a larger impact parameter, as shown in Fig. 2, while for peripheral collision with larger b, the number of participants decreased rapidly, and at approximately 6 fm, which is approximately equal to the radius of the nucleus of ^{197}Au in the Woods–Saxon model [37], leading to a more rapid decay for a larger impact parameter.

Studies on heavy-ion collision [9, 58] have revealed a global rotation system with large angular momentum. In Fig. 4, we showed the distribution of the average angular velocity along the *y*-axis ω_y in the rapidity-transverse momentum plane, which implied that most participants carried a small angular velocity of the order of magnitude of approximately 10^{-2}. Correspondingly, in the second panel of Fig. 3, for the collective behavior, the total system at the parton freeze-out state was estimated to have an average angular velocity approximately equal to 0.02 1/fm, where we discussed the case of a middle range of impact parameter at $b = 4.5$ fm.

In most panel of Fig.4, the range of ω_y distribution in rapidity at relatively high p_T was large compared to the low transverse momentum, although most of them remained around the mid-rapidity range. However, for the particles

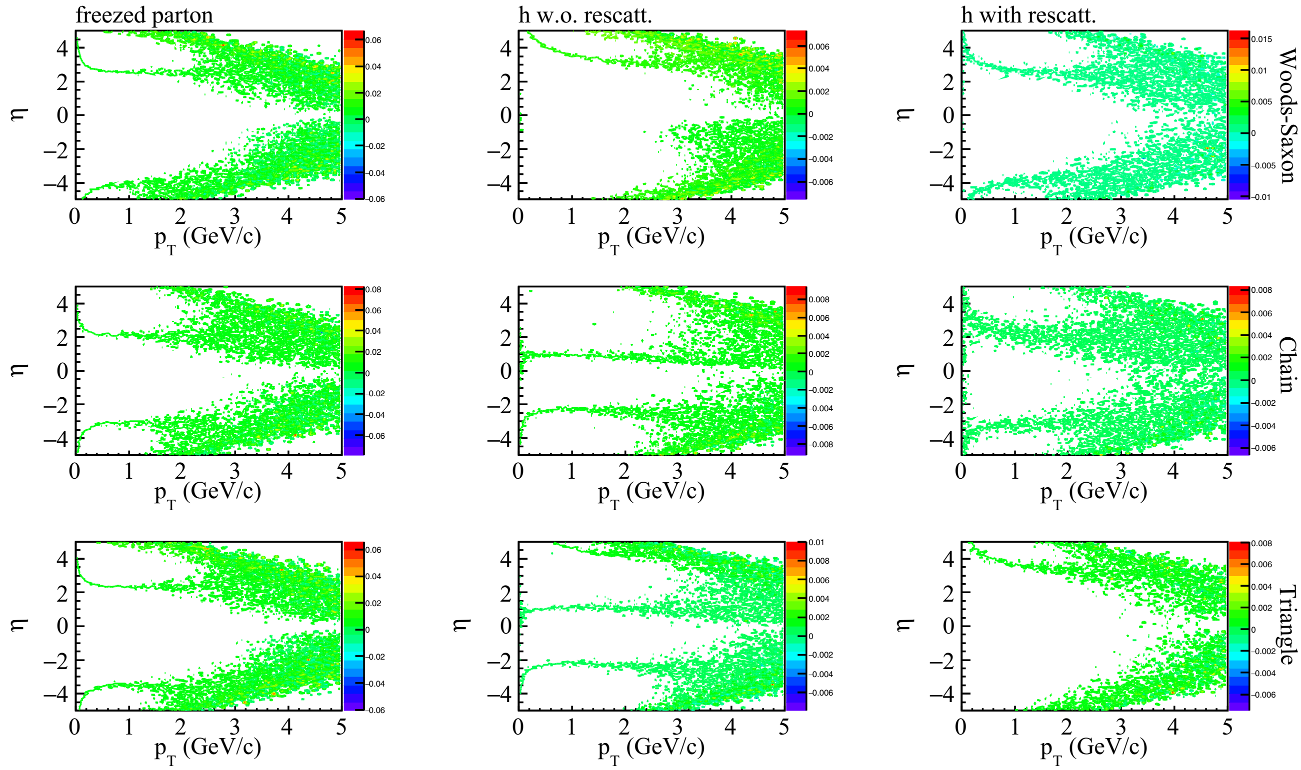

Fig. 4 (Color online) Angular velocity (ω_y) distribution along the y-axis in the transverse momentum (p_{T}) and rapidity (η) plane in $^{12}\mathrm{C}+^{197}\mathrm{Au}$ collision at $\sqrt{s_{\mathrm{NN}}}=200$ GeV. The impact parameter is $b=4.5$ fm for the mid-central collision. The left to right panels correspond to the freeze-out partons, the hadrons without hadronic rescattering, and the final-state hadrons, while from top to bottom are the three different α-clustering structures listed as the Woods–Saxon structure, the chain structure, and the triangle structure

with relatively lower transverse momentum, rapidity range was narrower and at a larger magnitude, implying a strong collective structure, which could probably be seen as collective flow [31, 51]. In addition, from the density distribution in Fig. 5, it can be seen that the center of collision region that composed of participants stayed with collective flow before being scattered out in the early stage.

In the scenario [31, 51], the ^{197}Au nucleus would move toward the negative direction along the rapidity axis, while ^{12}C took the opposite direction, which after collision transferred to a QGP matter and formed the global rotation [9]. In Fig. 5, for the impact parameter at 4.5 fm, most of the particle density was distributed in the range of low p_{T} and mid-rapidity in Fig. 5. In the left column of Fig. 5, the two most dense regions at the parton freeze-out state represent the original ^{12}C and ^{197}Au nucleus [19–23]. With time evolution, the two nuclei in opposite directions, which is shown in the middle panels, and their transverse momentum expanded toward a larger range. After the particles scattered out to the final-state hadrons, the system had a lower density that was chiefly distributed in the range of low p_{T} and mid-rapidity.

Comparing the left and the middle column of Fig. 4, the angular velocity ω_y moved toward the region of larger p_{T}, which manifested the expansion of the system. At the same time, the magnitude of ω_y decreases to 10^{-3}, which corresponds to the collective $\langle\omega_y\rangle$ in Fig. 3c, d. In the right column, some scattered hadrons at a higher p_{T} and rapidity obtained higher angular momentum, which consequently led to a larger ω_y. Few hadrons at large rapidity edge even carried large ω_y that represent the high velocity scattered particles at the edge of rotation.

In a previous work on the collective flow [51], we reported the configurations of Woods–Saxon distribution and two α-clustering distributions for ^{12}C to have very distinctive behaviors in the collective flow such as v_2 and v_3. However, in this study, for angular velocity, we found that the differences among the three structures were not as evident as the previous cases. For instance, global behaviors of the system such as I_0 and $\langle\omega_y\rangle$ in Figs. 2 and 3 perceived a rather small discrepancy among the three different cases of ^{12}C configuration. On the other hand, J_y seemed to show a more significant difference, where Woods–Saxon distribution possessed the largest angular momentum J_y, followed by the triangle clusters structure, and then the chain clusters. The discrepancy between Woods–Saxon distribution and chain could be as large as

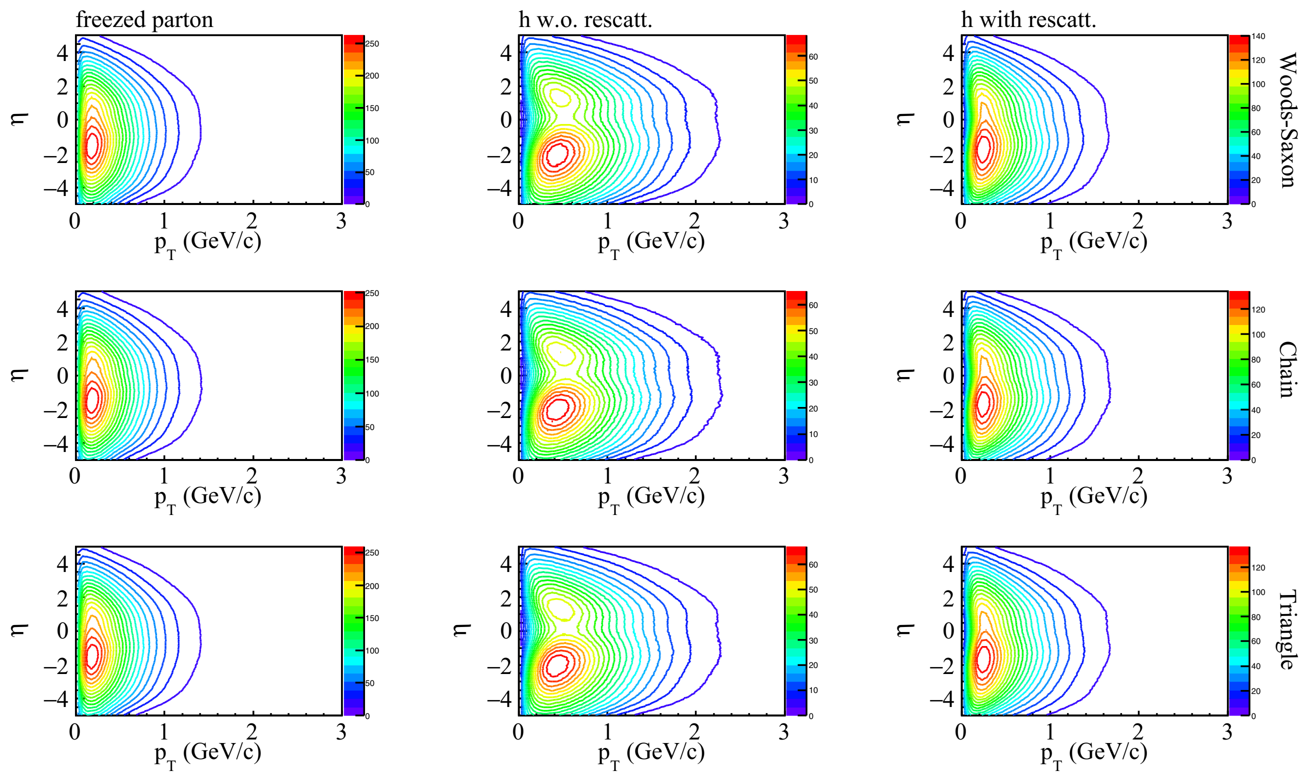

Fig. 5 (Color online) Same as Fig. 4 but for number density

approximately 20–30% at the peak, with an impact parameter equal to 6 fm. The internal configurations of α-cluster inside ^{12}C [33, 34] determined the initial geometry of the collision system. At and after the system phase transition, it is highly probable that such geometry remained in the system [51] and could be manifested in later evolvement. Even in the final state, shown in (d) of Fig. 1, the discrepancy of the angular momentum could be large as 20% at peak. However, because of the expansion for flow, the average speed of system was expected to gradually decrease, making the distinction difficult. It is much likely that more interesting mechanism could be suggested in physical behavior of collective behavior.

4 Summary

In summary, we simulated the collisions of ^{12}C against ^{197}Au at $\sqrt{s_{\rm NN}}$ = 200 GeV using AMPT model, where three different structure patterns of C were considered separately and compared. We found the effects on the angular momentum of the chain and triangle α-clustered cases as well as the Woods–Saxon distribution case to have a discrepancy. Other collective behaviors, including angular inertia and average angular velocity, were also examined and were found to have much less distinction. This is consistent with the density distribution and angular velocity distribution for the three patterns, suggesting possible analysis for experimental study.

References

1. L. Adamczyk, J.K. Adkins, G. Agakishiev et al., (STAR Collaboration), Beam-energy dependence of the directed flow of protons, antiprotons, and pions in Au + Au collisions. Phys. Rev. Lett. **112**, 162301 (2014). https://doi.org/10.1103/PhysRevLett.112.162301
2. L. Adamczyk, J.K. Adkins, G. Agakishiev, (STAR Collaboration), Elliptic flow of identified hadrons in Au + Au collisions at $\sqrt{s \text{ NN}}$ = 7.7–62.4 GeV. Phys. Rev. C **88**, 014902 (2013). https://doi.org/10.1103/PhysRevC.88.014902
3. L. Adamczyk, J.K. Adkins, G. Agakishiev et al., (STAR Collaboration), Third harmonic flow of charged particles in Au + Au collisions at $\sqrt{s \text{ NN}}$ = 200 GeV. Phys. Rev. C **88**, 014904 (2013). https://doi.org/10.1103/PhysRevC.88.014904
4. L. Adamczyk, J.K. Adkins, G. Agakishiev et al., (STAR Collaboration), Observation of charge asymmetry dependence of pion elliptic flow and the possible chiral magnetic wave in heavy-ion collisions. Phys. Rev. Lett. **114**, 252302 (2015). https://doi.org/10.1103/PhysRevLett.114.252302
5. J. Adams, C. Adler, M.M. Aggarwal et al., (STAR Collaboration), Evidence from d + Au measurements for final-state suppression of high-p_T hadrons in Au + Au collisions at RHIC. Phys. Rev. Lett. **91**, 072304 (2003). https://doi.org/10.1103/PhysRevLett.91.072304

6. J. Adams, C. Adler, M.M. Aggarwal et al., (STAR Collaboration), Transverse-momentum and collision-energy dependence of high-p_T hadron suppression in Au + Au collisions at ultrarelativistic energies. Phys. Rev. Lett. **91**, 172302 (2003). https://doi.org/10.1103/PhysRevLett.91.172302
7. L. Adamczyk, J.K. Adkins, G. Agakishiev et al., (STAR Collaboration), Beam-energy-dependent two-pion interferometry and the freeze-out eccentricity of pions measured in heavy ion collisions at the STAR detector. Phys. Rev. C **92**, 014904 (2015). https://doi.org/10.1103/PhysRevC.92.014904
8. A. Adare, et al. (PHENIX Collaboration), Beam-energy and system-size dependence of the space-time extent of the pion emission source produced in heavy ion collisions (2014). arXiv:1410.2559
9. Y. Jiang, Z.-W. Lin, J. Liao, Rotating quark-gluon plasma in relativistic heavy-ion collisions. Phys. Rev. C **94**, 044910 (2016). https://doi.org/10.1103/PhysRevC.94.044910
10. Z.-T. Liang, X.-N. Wang, Globally polarized quark-gluon plasma in noncentral $A+A$ collisions. Phys. Rev. Lett. **94**, 102301 (2005). https://doi.org/10.1103/PhysRevLett.94.102301
11. X.-G. Huang, P. Huovinen, X.-N. Wang, Quark polarization in a viscous quark-gluon plasma. Phys. Rev. C **84**, 054910 (2011). https://doi.org/10.1103/PhysRevC.84.054910
12. A.H. Tang, B. Tu, C.S. Zhou, Practical considerations for measuring global spin alignment of vector mesons in relativistic heavy ion collisions. Phys. Rev. C **98**, 044907 (2018). https://doi.org/10.1103/PhysRevC.98.044907
13. Z.-T. Liang, X.-N. Wang, Spin alignment of vector mesons in non-central A + A collisions. Phys. Lett. B **629**, 20–26 (2005). https://doi.org/10.1016/j.physletb.2005.09.060
14. L. Adamczyk et al., (STAR Collaboration), Global Λ hyperon polarization in nuclear collisions. Nature **541**, 62–65 (2017). https://doi.org/10.1038/nature23004
15. R.D. de Souza, J. Takahashi, T. Kodama et al., Effects of initial state fluctuations in the final state elliptic flow measurements using the NeXSPheRIO model. Phys. Rev. C **85**, 054909 (2012). https://doi.org/10.1103/PhysRevC.85.054909
16. A. Chaudhuri, Fluctuating initial conditions and fluctuations in elliptic and triangular flow. Phys. Lett. B **710**, 339–342 (2012). https://doi.org/10.1016/j.physletb.2012.02.067
17. H. Song, S.A. Bass, U. Heinzi, Elliptic flow in $\sqrt{s}$ = 200 GeV Au + Au collisions and $\sqrt{s}$ = 2.76 TeV Pb + Pb collisions: insights from viscous hydrodynamics + hadron cascade hybrid model. Phys. Rev. C **83**, 054912 (2011). https://doi.org/10.1103/PhysRevC.83.054912
18. S. Floerchinger, U.A. Wiedemann, Mode-by-mode fluid dynamics for relativistic heavy ion collisions. Phys. Lett. B **728**, 407–411 (2014). https://doi.org/10.1016/j.physletb.2013.12.025
19. P. Bozek, W. Broniowski, E.R. Arriola, α clusters and collective flow in ultrarelativistic carbon-heavy-nucleus collisions. Phys. Rev. C **064902**, 90 (2014). https://doi.org/10.1103/PhysRevC.90.064902
20. W. Broniowski, E.R. Arriola, Signatures of α clustering in light nuclei from relativistic nuclear collisions. Phys. Rev. Lett. **112**, 112501 (2014). https://doi.org/10.1103/PhysRevLett.112.112501
21. L. Ma, G.L. Ma, Y.G. Ma, Initial partonic eccentricity fluctuations in a multiphase transport model. Phys. Rev. C **94**, 044915 (2016). https://doi.org/10.1103/PhysRevC.94.044915
22. L. Ma, G.L. Ma, Y.G. Ma, Anisotropic flow and flow fluctuations for Au + Au at $\sqrt{s_{NN}} = 200$ GeV in a multiphase transport model. Phys. Rev. C **89**, 044907 (2014). https://doi.org/10.1103/PhysRevC.89.044907
23. L.X. Han, G.L. Ma, Y.G. Ma et al., Initial fluctuation effect on harmonic flows in high-energy heavy-ion collisions. Phys. Rev. C **84**, 064907 (2011). https://doi.org/10.1103/PhysRevC.84.064907
24. H.-C. Song, Y. Zhou, K. Gajdosova, Collective flow and hydrodynamics in large and small systems at the LHC. Nucl. Sci. Technol. **28**, 99 (2017). https://doi.org/10.1007/s41365-017-0245-4
25. J. Wang, Y.G. Ma, G.Q. Zhang, Initial fluctuation effect on elliptic flow in Au + Au collision at 1 GeV/A. Nucl. Sci. Technol. **24**, 030501 (2013). https://doi.org/10.13538/j.1001-8042/nst.2013.03.004
26. C.C. Guo, W.B. He, Y.G. Ma, Collective flows of ^{16}O + ^{16}O collisions with α-clustering configurations. Chin. Phys. Lett. **34**, 092101 (2017). https://doi.org/10.1088/0256-307X/34/9/092101
27. X.-F. Luo, N. Xu, Search for the QCD critical point with fluctuations of conserved quantities in relativistic heavy-ion collisions at RHIC: an overview. Nucl. Sci. Technol. **28**, 112 (2017). https://doi.org/10.1007/s41365-017-0257-0
28. X. Jin, J. Chen, Z. Lin et al., Explore the QCD phase transition phenomena from a multiphase transport model. Sci. China Phys. Mech. **62**, 11012 (2018). https://doi.org/10.1007/s11433-018-9272-4
29. C.M. Ko, F. Li, Density fluctuations in baryon-rich quark matter. Nucl. Sci. Technol. **27**, 140 (2016). https://doi.org/10.1007/s41365-016-0141-3
30. Q.Y. Shou, G.L. Ma, Y.G. Ma, Charge separation with fluctuating domains in relativistic heavy-ion collisions. Phys. Rev. C **90**, 047901 (2014). https://doi.org/10.1103/PhysRevC.90.047901
31. S. Zhang, Y.G. Ma, J.H. Chen et al., Nuclear cluster structure effect on elliptic and triangular flows in heavy-ion collisions. Phys. Rev. C **95**, 064904 (2017). https://doi.org/10.1103/PhysRevC.95.064904
32. F.D. Murnaghan, Review: G. Gamow, constitution of atomic nuclei and radioactivity. Bull. Amer. Math. Soc. **39**, 487 (1993)
33. W.B. He, Y.G. Ma, X.G. Cao et al., Giant dipole resonance as a fingerprint of α clustering configurations in ^{12}C and ^{16}O. Phys. Rev. Lett. bf **113**, 032506 (2014). https://doi.org/10.1103/PhysRevLett.113.032506
34. W.B. He, Y.G. Ma, X.G. Cao et al., Dipole oscillation modes in light α-clustering nuclei. Phys. Rev. C **94**, 014301 (2016). https://doi.org/10.1103/PhysRevC.94.014301
35. B.S. Huang, Y.G. Ma, W.B. He, Photonuclear reaction as a probe for α-clustering nuclei in the quasi-deuteron region. Phys. Rev. C **95**, 034606 (2017). https://doi.org/10.1103/PhysRevC.95.034606
36. B.S. Huang, Y.G. Ma, W.B. He, Alpha-clustering effects on ^{16}O $(4\gamma,\ np)^{14}$N in quasi-deuteron region. Eur. Phys. J. A **53**, 119 (2017)
37. Z.-W. Lin, C.M. Ko, B.-A. Li et al., Multiphase transport model for relativistic heavy ion collisions. Phys. Rev. C **72**, 064901 (2005). https://doi.org/10.1103/PhysRevC.72.064901
38. G.-L. Ma, Z.-W. Lin, Predictions for $\sqrt{s_{NN}} = 5.02$ TeV Pb + Pb collisions from a multiphase transport model. Phys. Rev. C **93**, 054911 (2016). https://doi.org/10.1103/PhysRevC.93.054911
39. Z.-W. Lin, C.M. Ko, S. Pal, Partonic effects on pion interferometry at the relativistic heavy-ion collider. Phys. Rev. Lett. **89**, 152301 (2002). https://doi.org/10.1103/PhysRevLett.89.152301
40. B.I. Abelev, M.M. Aggarwal, Z. Ahammed et al., (STAR Collaboration), System-size independence of directed flow measured at the BNL relativistic heavy-ion collider. Phys. Rev. Lett. **101**, 252301 (2008). https://doi.org/10.1103/PhysRevLett.101.252301
41. A. Bzdak, G.-L. Ma, Elliptic and triangular flow in *p*–Pb and peripheral Pb–Pb collisions from parton scatterings. Phys. Rev. Lett. **113**, 252301 (2014). https://doi.org/10.1103/PhysRevLett.113.252301
42. G.-L. Ma, S. Zhang, Y.-G. Ma et al., Di-hadron azimuthal correlation and Mach-like cone structure in a parton/hadron transport model. Phys. Lett. B **641**, 362–367 (2006)

43. X.-H. Jin, J.-H. Chen, Y.-G. Ma, Ω and ϕ production in Au + Au collisions at =11.5 and 7.7 GeV in a dynamical quark coalescence model. Nucl. Sci. Technol. **29**(2), 54 (2018). https://doi.org/10.1007/s41365-018-0393-1
44. K. Hattori, X.-G. Huang, Novel quantum phenomena induced by strong magnetic fields in heavy-ion collisions. Nucl. Sci. Technol. **28**, 26 (2017)
45. X.-L. Zhao, Y.-G. Ma, G.-L. Ma, Electromagnetic fields in small systems from a multiphase transport model. Phys. Rev. C **97**, 024910 (2018). https://doi.org/10.1103/PhysRevC.97.024910
46. X.-N. Wang, M. Gyulassy, HIJING: a Monte Carlo model for multiple jet production in pp , pA , and AA collisions. Phys. Rev. D **44**, 3501–3516 (1991). https://doi.org/10.1103/PhysRevD.44.3501
47. M. Gyulassy, X.-N. Wang, HIJING 1.0: a Monte Carlo program for parton and particle production in high energy hadronic and nuclear collisions. Comput. Phys. Commun. **83**, 307 (1994). https://doi.org/10.1016/0010-4655(94)90057-4
48. B. Zhang, ZPC 1.0.1: a parton cascade for ultrarelativistic heavy ion collisions. Comput. Phys. Commun. **109**, 193–206 (1998)
49. B.-A. Li, C.M. Ko, Formation of superdense hadronic matter in high energy heavy-ion collisions. Phys. Rev. C **52**, 2037–2063 (1995). https://doi.org/10.1103/PhysRevC.52.2037
50. T. Maruyama, K. Niita, A. Iwamoto, Extension of quantum molecular dynamics and its application to heavy-ion collisions. Phys. Rev. C **53**, 297–304 (1996). https://doi.org/10.1103/PhysRevC.53.297
51. S. Zhang, Y.G. Ma, J.H. Chen et al., Collective flows of α-clustering ^{12}C $+^{197}$ Au by using different flow analysis methods. Eur. Phys. J. A **54**, 161 (2018). https://doi.org/10.1140/epja/i2018-12597-y
52. S.A. Voloshin, A.M. Poskanzer, A. Tang et al., Elliptic flow in the Gaussian model of eccentricity fluctuations. Phys. Lett. B **659**, 537–541 (2008). https://doi.org/10.1016/j.physletb.2007.11.043
53. B. Alver, G. Roland, Collision-geometry fluctuations and triangular flow in heavy-ion collisions. Phys. Rev. C **81**, 054905 (2010). https://doi.org/10.1103/PhysRevC.81.054905
54. R.A. Lacey, R. Wei, J. Jia et al., Initial eccentricity fluctuations and their relation to higher-order flow harmonics. Phys. Rev. C **83**, 044902 (2011). https://doi.org/10.1103/PhysRevC.83.044902
55. Y.G. Ma, W.Q. Shen, Z.Y. Zhu, Collective motions of reverse reaction system in the intermediate energy domain via the quantum molecular dynamics approach. Phys. Rev. C **51**, 1029 (1995). https://doi.org/10.1103/PhysRevC.51.1029
56. L. He, T. Edmonds, Z.-W. Lin et al., Phys. Lett. B **753**, 506–510 (2016). https://doi.org/10.1016/j.physletb.2015.12.051
57. G.-L. Ma, A. Bzdak, Flow in small systems from parton scatterings. Nucl. Phys. A **956**, 745–748 (2016). https://doi.org/10.1016/j.nuclphysa.2016.01.057
58. W.-T. Deng, X.-G. Huang, Vorticity in heavy-ion collisions. Phys. Rev. C **93**, 064907 (2016). https://doi.org/10.1103/PhysRevC.93.064907